Monolithic IPMC Fins for Propulsion and Maneuvering in Bioinspired Underwater Robotics

Joel J. Hubbard, Maxwell Fleming, Viljar Palmre, David Pugal, Kwang J. Kim, and Kam K. Leang, *Member, IEEE*

Abstract—Emerging bioinspired underwater systems, such as autonomous ocean mapping and surveillance vehicles, that maneuver through their environment by mimicking the swimming motion of aquatic animals, can benefit from soft monolithic actuators and control surfaces capable of undergoing complex deformations. Herein, an electrically driven ionic polymer–metal composite (IPMC) artificial muscle with uniquely patterned electrodes for creating complex deformations is presented. The surface electrode pattern on the IPMC is created using a simple surface machining process. By selectively activating specific regions of the IPMC, bending, twisting, flapping, and other bioinspired locomotive behavior can be achieved. For instance, the bending and twisting response of an example 50 mm × 25 mm × 0.5 mm patterned IPMC actuator is characterized to determine its range of motion, output force and torque, as well as its effectiveness as a fish-fin-like propulsor. The experimental results show that the twisting angle exceeds 8°; the blocking tip force and torque can be as high as 16.5 mN (at 3 V) and 0.83 N · mm (at 4 V), respectively (driven at 0.05 Hz); and an average thrust force of approximately 0.4 mN (driven by 4-V sinusoidal input at 1 Hz) can be generated. These newly developed IPMC fins can be exploited to create novel and efficient propulsors for next-generation underwater robotic vehicles. An example bioinspired robotic fish is presented which exploits the capabilities of the patterned IPMCs for propulsion and maneuvering, where an average maximum swimming speed of approximately 28 mm/s is reported.

Index Terms—Ionic polymer metal composite actuators, propulsion and maneuvering, UAVs, underwater robotics.

I. INTRODUCTION

IN recent years, the superior maneuvering and swimming capabilities of marine animals over man-made underwater vehicles have attracted significant attention for bioinspired

J. J. Hubbard and K. K. Leang are with the Electroactive Systems and Controls Laboratory, University of Nevada—Reno, Reno, NV 89557-0312 USA (e-mail: kam@unr.edu).

M. Fleming was with Electroactive Systems and Controls Laboratory, University of Nevada—Reno, Reno, NV 89557-0312 USA. He is now with Novartis Consumer Health, Inc., Waverly, NE 68462 USA.

V. Palmre and D. Pugal are with the Active Materials and Processing Laboratory, Department of Mechanical Engineering, University of Nevada–Reno, Reno, NV 89557-0312 USA.

K. J. Kim is with the Active Materials and Processing Laboratory, Department of Mechanical Engineering, University of Nevada—Reno, Reno, NV 89557-0312 USA and also with the University of Nevada—Las Vegas, Las Vegas, NV 89154-4027 USA.

Color versions of one or more of the figures in this paper are available online at http://ieeexplore.ieee.org.

Digital Object Identifier 10.1109/JOE.2013.2259318

designs [1], [2]. However, to mimic the performance of even the simplest of these animals, the control surfaces for man-made robotic systems must have multiple degrees of freedom, allowing for a combination of bending, twisting, and other complex motions. Conventional actuators, though, such as direct current (dc) servos, magnetic drives, and pneumatic pistons generally offer single degree-of-freedom motion. High degrees-of-freedom motion is often achieved using multiple actuators coupled with complex mechanisms. Unfortunately, the increase in complexity also increases the propulsion system's footprint as well as weight and cost. Also, current techniques for underwater locomotion that utilize propellers have significant disadvantages when used to generate small forces for maneuvering [3]. Herein, an ionic polymer–metal composite (IPMC) artificial muscle fin with uniquely patterned electrodes for creating complex deformations is presented. The IPMC material is a promising active ("smart") material for engineering novel soft biomimetic actuators and sensors, particularly for underwater autonomous vehicles (UAVs) and related applications [4]–[8]. An IPMC consists of a neutralized ionomeric membrane sandwiched between noble metals (such as platinum), which serve as electrodes. Notable advantages of IPMCs include low driving voltage (<5 V), relatively large strain, soft and flexible structure, and the ability to operate in an aqueous environment (such as water). When an IPMC is mechanically deformed, charge redistribution within the material enables it to function as a sensor [8], [9]. The IPMCs are typically used as bending actuators with one end fixed. Proposed herein are IPMC fins with sectored (patterned) electrodes, where the surface electrode material is sectored into different electrically isolated regions for generating complex deformation. Due to their ability for mechanoelectrical transduction, with careful design of the electrode pattern, certain areas of the IPMC can be used to create a highly deformable control surface, while at the same time other regions can be patterned for sensing fin deformation and responses to external stimulation [10]. The result is a compact monolithic control surface with integrated sensing for multifunctional applications. Electroactive polymer actuators have been created with similar capabilities [11]–[15]; however, the contribution of this work is the characterization and application of patterned IPMCs for maneuvering and propulsion in underwater autonomous systems. Specifically, this study examines the capabilities of a sectored IPMC, and the results can be applied to future analysis and design of bioinspired underwater robotic systems.

IPMC-based actuators have previously been integrated into robotic systems to emulate the movement of fish [16]–[24], jellyfish [25], and manta rays [26], [27]. Other aquatic designs have also been explored, including a snake [28], a hovering

microswimmer [29], and an underwater walking microrobot [30]. These works served as proofs of concept for a handful of IPMC-based aquatic system designs, and several explored the swimming capabilities in a parametric fashion. For example, variables such as flapping frequency and fin geometry have been compared to performance attributes like swimming speed and thrust for simple fish robots using an IPMC as a caudal fin [16]–[18], [21], [24]. Swimming characteristics have also been explored for more complex systems which utilize multiple IPMCs. The effect of input frequency, wave number, and phase shift between actuators has been related to swimming speed, thrust, power consumption, and fin twist angle [27], [28], [31]. The work herein explores a similar set of input/output relationships. Setting this work apart, however, is the focus on sectored (patterned) IPMCs, as opposed to systems composed of either a single IPMC (which can produce simple bending motion) or multiple IPMCs which are mechanically connected.

In the following, a thorough experimental study is performed on IPMC fins with sectored electrodes for propulsion and maneuvering. Specifically, the achievable twisting/bending response, blocking force and torque, propulsion characteristics, and power consumption and effectiveness are measured and evaluated. These results can be utilized to guide the design of practical marine systems controlled by IPMC actuators. The monolithic IPMC-based caudal and pectoral fins are capable of generating bending and twisting motion for maneuvering while still producing ostraciiform swimming motion [32]. As an illustrative example, a bioinspired underwater robot is designed and outfitted with the sectored IPMC fins to serve as the pectoral and caudal fins. It should be noted that while the focus of this work is the application of sectored IPMCs to swimming robots, the characteristics studied can also be used for other fluid manipulation applications, such as multifunctional valves or pumps, similar to those proposed in [6].

The remainder of this paper is organized as follows. Section II briefly describes the fabrication process for creating the sectored IPMC fins. The design and modeling of the robotic platform which uses the IPMC fins is described in Section III. Afterwards, the characterization of IPMC fins is discussed in Section IV. The performance of the robotic fish which uses the IPMC fins is presented in Section V. Finally, concluding remarks are found in Section VI.

II. FABRICATION PROCESS

A. Electrode Plating and Patterning Process

The IPMC fin actuators (propulsors) are created from 0.5-mm-thick prefabricated perfluorosulfonic acid membrane. The 0.5-mm thickness is chosen to achieve a good balance between deflection and actuation force [5]. The IPMC fabrication process consists of three parts, the first being a conditioning process to clean the sample for electroless plating. Next, the sample is soaked in a platinum complex solution, tetraamine-platinum (II) chloridemonohydrate ($[Pt(NH_3)_4]Cl_2H_2O$), for several hours. The platinum is then metalized on the membrane surface via a reduction process to create electrodes on the polymer membrane. The IPMC propulsor is then cleaned in successive baths of sulfuric acid (H_2SO_4) and deionized (DI) water, and the reduction and cleaning processes are repeated
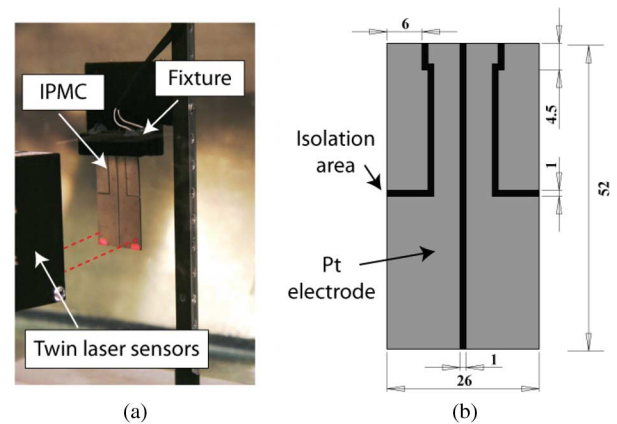

Fig. 1. (a) An experimental setup for measuring bending/twisting response for (b) an example patterned IPMC (units in millimeters).
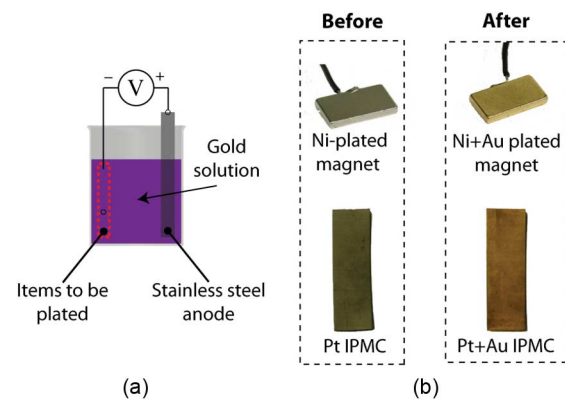

Fig. 2. Electrodeposition process for gold plating magnets and IPMCs.

until a sufficiently low surface resistance is achieved [5]. Last, the IPMC is hydrated with a salt solution to introduce mobile cations (in this case Li^+) in a process known as ion exchange.

Patterning of the electrodes is done using a computer-controlled milling machine equipped with a microsurface routing end mill [14], [15]. The end mill rotates at approximately 3000 rev/min and is programmed to follow a predefined trajectory which defines the electrode pattern. The end mill removes the metalized surface to a depth of 25–50 μm, exposing the underlying membrane. The end product is a monolithic IPMC with isolated electrodes, as illustrated in Fig. 1(b). Fig. 1(a) shows the experimental setup using two laser displacement sensors to measure the motion.

B. Electrical Contact Considerations and Gold Electroplating

The electrical contact system must be carefully designed for underwater applications. Stainless steel and copper clamps or conductive glues are typically used to establish an electrical connection between the power supply and the IPMC electrode [33]–[35]. Conductive glue can be an effective method of connecting wires, but prolonged submersion in water may be undesirable and a separate clamping mechanism still must be devised to hold the actuator in place. Certain grades of stainless steel can be used as a contact material and provide great corrosion resistance, but the material can be difficult to solder and must still be
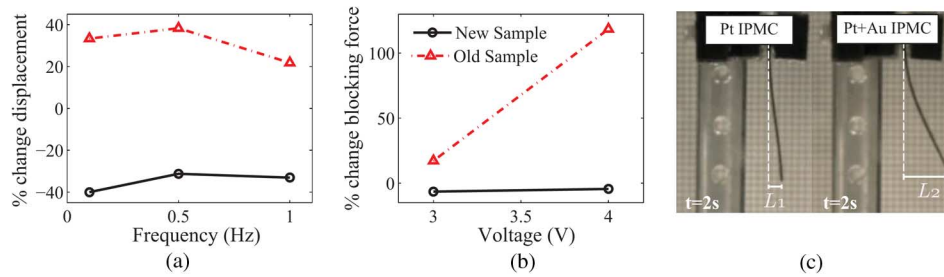
Fig. 3. (a) Displacement and (b) force responses before and after gold plating. (c) IPMC bending before (left) and after (right) gold plating.

integrated into a mechanical clamping system. Copper's superior conductivity is ideal, but its low corrosion resistance makes submersion in water a problem. In [33], copper electrodes were sputter coated with platinum to prevent corrosion and any chemical reaction between the surface of the IPMC and the electrode.

There is a need for a simple mechanism and contact material to make good electrical contact with the IPMC actuator. An all-inclusive design incorporating nickel plated neodymium magnets is proposed in [36]. Similarly, in this work, strong nickel plated rare earth neodymium magnets (NdFeB) are used as a multifunctional solution for clamping and power delivery. The magnets make for an easily removable clamp with a high clamping force of 1.8–3.6 N [0.4–0.8 pound-force (lbf)]. The magnets used are typically electroplated with nickel and copper in the order Ni–Cu–Ni with each layer being approximately 5–7 μm thick. The magnets are quite modular in that they can easily be replaced or expanded by adding adjacent magnets.

The nickel coating is easily soldered to and is corrosion resistant. However, it is found that after prolonged submersion in water under an applied potential, breakdown of both the neodymium magnets' nickel surface and the IPMCs' platinum surface occurs due to the creation of a galvanic cell. This is exacerbated by the presence of voids in the nickel surface that expose the underlying copper layer and expedite the process. The differences in anodic potential between the platinum surface of the IPMC actuator and the magnet's nickel–copper surface can lead to degradation of the electrical contact through a chemical reduction of the platinum. To combat this problem, the nickel plated magnets are electroplated utilizing a high-quality gold plating solution to form a 1–2-μm-thick layer of gold on the magnet's surface. The electroplating process is carried out as follows. First, the neodymium magnet contacts are attached to a negative lead (cathode) and placed in a gold solution (see Fig. 2). A positive lead (anode) is connected to a strip of stainless steel, which is also placed in the solution, and a potential is applied. In the electrodeposition process, the thickness of the resulting gold layer is determined by the current density and immersion time. The nickel layer on the magnets acts as a barrier and slows the diffusion of copper atoms into the gold while the gold layer's low anodic potential minimizes the electrochemical reactions that damage the IPMC's platinum electrode. This process of electroplating gold onto the magnet's surface can also be applied to plate gold onto the electrodes of an IPMC to enhance its performance, as described next.

Performance degradation of the IPMC actuators can occur over time from the loss of mobile Li^+ cations as well as an increase in surface (electrode) resistance. The latter is a result of the platinum electrode surface developing cracks or voids from high levels of actuation or dehydration. The characteristics of degradation is challenging to quantify since performance can vary significantly from one sample to the next. The parameters of an individual sample (i.e., membrane thickness, electrode thickness, electrode composition, cation, etc.) certainly influence a sample's resistance to degradation, but even seemingly identical samples can behave quite differently. To give a very general idea of the process though, several observations were made for the samples used in this work. When actuated out of water, dehydration leads to quick degradation in performance, with a time scale on the order of minutes. Further, repeated dehydration and rehydration accelerates the overall degradation process, likely by repeatedly expanding and contracting the electrode layers. If a sample is subjected to dc voltages above the electrolysis point (approximately 1.8 V), the membrane can be damaged and stiffened in a matter of seconds. However, if an alternating current is applied at a high enough frequency, the IPMC is more resilient at higher voltages. Under normal conditions (sufficiently low voltage and well hydrated), the IPMC's deflection will reduce significantly over the course of a day of testing, however, a nearly full recovery can be seen when the actuator is allowed to rest overnight. Quick electroplating of gold to fill the voids in the electrode layers and lower the surface resistance can "resurrect" damaged IPMCs and improve performance. To demonstrate the effect of gold plating, a newly fabricated and an old, poorly performing IPMC were electroplated with gold using the previously described process (see Fig. 2). The newly fabricated IPMC had a surface resistance (measured by the two-point probe method) of 0.48 and 0.26 Ω/cm before and after gold plating, respectively, while the old sample had resistances of 2.82 and 0.28 Ω/cm before and after gold plating, respectively. The tip deflection and blocking force of the IPMCs were also tested before and after the plating process, and the percent change after plating is shown in Fig. 3(a) and (b). The performance of an old sample that is rejuvenated by the gold plating process is shown qualitatively in Fig. 3(c). The results show that gold electroplating is beneficial for old samples with degraded performance; both the displacement and blocking force are significantly improved. In the case of a new sample with already good performance and low electrode resistance, nearly no improvement is observed after electroplating.
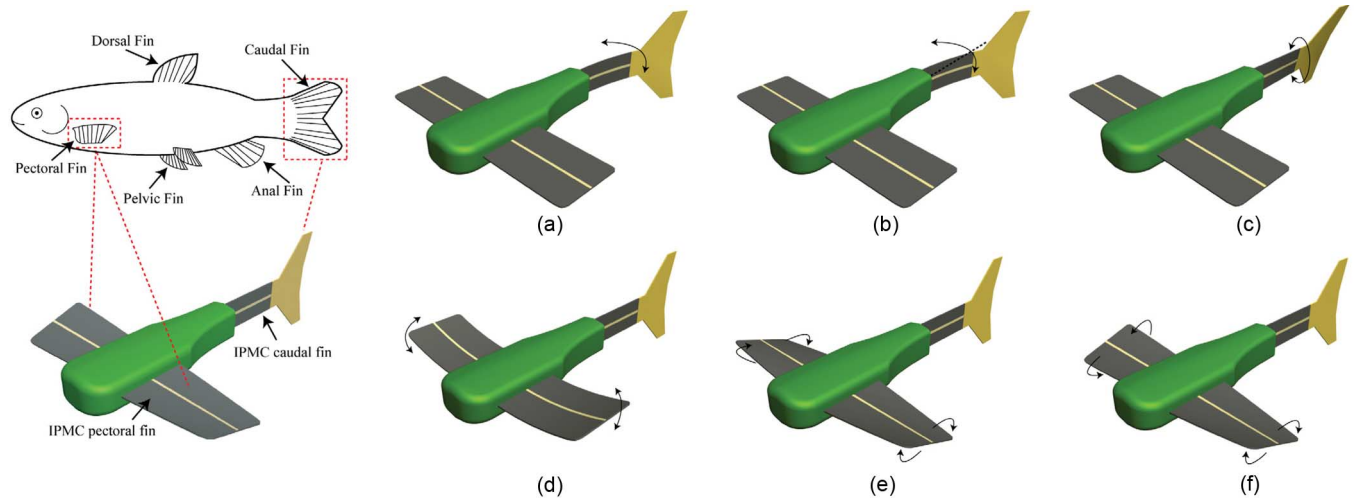
Fig. 4. A typical fish and illustration of the robotic platform driven by IPMC fins and possible maneuvering capabilities. (a) Caudal fin bending "thrust generation"; (b) caudal fin bending (nonneutral axis) "yaw"; (c) caudal fin twisting " roll/banking"; (d) pectoral fin bending "translation/roll/banking"; (e) pectoral fin twisting "pitch-dive/surface"; and (f) pectoral fin twisting "roll."

III. DESIGN OF BIOINSPIRED ROBOTIC FISH

A. Mechanical Design

A bioinspired robotic system (platform) is designed to take advantage of the patterned IPMC fin. Fish typically have seven active surfaces, the fins, as shown in Fig. 4. They feature varying degrees of activity in propulsion and maneuvering, and the functions of the same fin varies from fish to fish. For example, the bluegill sunfish has an incredible level of maneuverability, due almost entirely to the motion of the pectoral fins. The motion is undulatory and very complex, and if it were decomposed into the component modes, the first five modes together would comprise only about 80% of the total fin motion [37]. Being so dependent on the pectoral fins, the maneuvering and locomotion of this fish would be characterized as median and/or paired fin (MPF) locomotion, as opposed to body and/or caudal fin (BCF) locomotion. Fish that utilize MPF or BCF locomotion can be further categorized based on whether the movements are more oscillatory or undulatory. Highly undulatory fish utilizing BCF locomotion (such as an eel) are said to exhibit anguilliform swimming [38]. The motion of either of these fish would be admittedly difficult to replicate using patterned IPMCs. Although sectoring the IPMCs produces additional degrees of freedom, they still might be ineffective at reproducing this highly undulatory motion. On the other side of the BCF spectrum, however, is ostraciiform swimming, in which the caudal fin alone oscillates. One example of a fish using ostraciiform swimming is the boxfish. Simple IPMCs have already been used to reproduce this kind of swimming [17]–[21], but surely sectored IPMCs can be used to reach further into the spectrum of swimming modes, reproducing somewhat more undulatory motions.

While all of the fins of a fish can be useful, the fins that are most active in a wide range of fish locomotion regimes are the pectoral and caudal fins. The other fins are primarily for stability and as such, are less relevant to realizing biomimetic locomotion and the associated advantages. A comparison between a fish and the robotic platform is shown in Fig. 4, where the patterned IPMCs are used for the pectoral and caudal fins. The possible

maneuvering capabilities of the platform are depicted in Fig. 4. As shown, the pectoral fins act as a control surface, the twist angle of which determines the range of maneuverability, including the amount of lift, dive, and turning/banking. The caudal fin functions as the primary source of thrust for propelling the robot forward.

B. Body Dynamics

A model for the body dynamics of an underwater robot is proposed and experimentally validated in [34]. This model is adapted and used in this work to model the dynamics of the robotic fish with ostraciiform locomotion swimming. To simplify the notation, time dependence on some variables is omitted.

The robot platform is modeled relative to a Newtonian reference frame defined by a set of Cartesian coordinates X, Y, Z, as shown in Fig. 5(a). Additionally, a fixed Cartesian coordinate system centered about the body's center of buoyancy is illustrated and defined by x, y, z. Several assumptions are made in forming the model.

1) The robot's center of mass and center of buoyancy are coincident.
2) The entire body displaces its own weight in water, i.e., it is neutrally buoyant.
3) Only in-plane motion (x/y-plane), yaw, w (rotation about the Z-axis), surge, v (forward motion in x-direction), and sway, u (transverse motion in y-direction) are relevant to vehicle behavior.
4) Yaw (w), surge (v), and sway (u) motions do not exhibit inertial coupling (i.e., the movements are decoupled).
5) The robot's body, for hydrodynamic purposes, can be approximated by a prolate spheroid.

The position of the platform in the inertial reference frame is illustrated in Fig. 5(a). The external forces acting on the body are also depicted. The velocity vector is denoted by V, where the magnitude of the vector is $\bar{V} = \sqrt{v^2 + u^2}$. In the figure, four angles, θ, α, β and ϕ, are defined. The angle θ represents the oscillation angle of the caudal fin with respect to the x-axis.
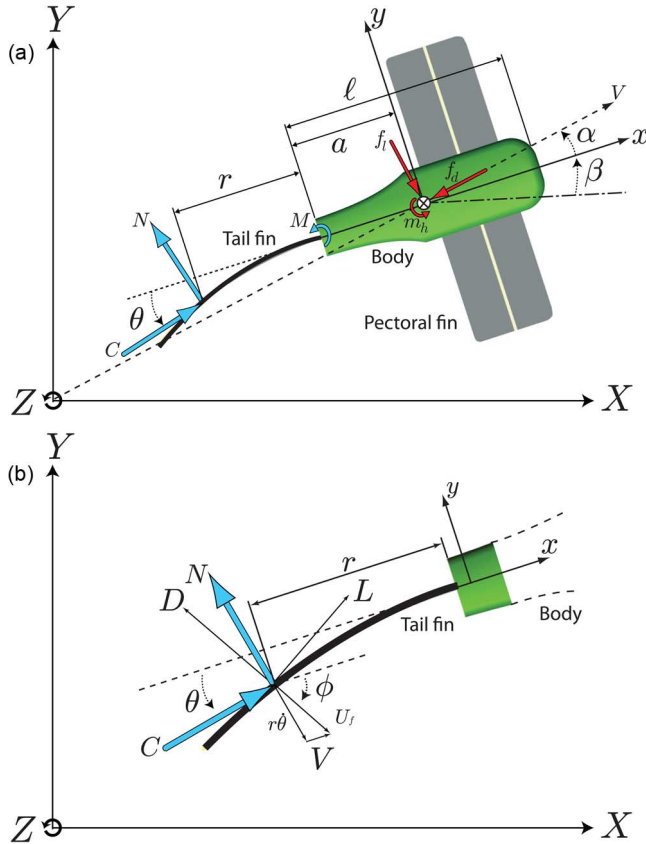
Fig. 5. Free body diagrams: (a) the 2-D representation of the body dynamics of the platform during ostraciiform locomotion and (b) the free body diagram of forces acting on oscillating tail, where D and L represent drag and lift forces, respectively.

The attack angle α is the angle formed by the velocity vector V and the x-axis. The angle β is the platform's attitude relative to the frame of reference; this orientation represents the yaw angle of the robot and when $\beta = 0$, the X and x-axes are parallel. Last, the fourth angle ϕ is the attack angle of the tail fin and is addressed in Section III-C.

The Eulerian description of the swimming robot's planar motion is expressed by the following system equations [17], [34]:

$$\frac{dv}{dt} = \frac{F_x + (m_b - Y_{\dot{u}})uw}{m_b - X_{\dot{v}}} \quad (1)$$

$$\frac{du}{dt} = \frac{F_y - (m_b - X_{\dot{v}})vw}{m_b - Y_{\dot{u}}} \quad (2)$$

$$\frac{dw}{dt} = \frac{(Y_{\dot{u}} - X_{\dot{v}})vu + M_z}{J_z - K_{\dot{w}}}. \quad (3)$$

The mass of the vehicle and its moment of inertia about the z-axis are denoted by m_b and J_z, respectively. The hydrodynamic variables $Y_{\dot{u}}$, $X_{\dot{v}}$, and $K_{\dot{w}}$ are defined in [39] to account for the added mass on the robot due to hydrodynamic effects.

Equations (1)–(3) feature the force variables F_x and F_y and moment M_z. These represent the sum of the external forces acting on the body in the x- and y-directions and the moments

about the z-axis. These loads represent those generated in reaction to the IPMC actuator's movement as well as forces due to hydrodynamic dampening, and they are given by

$$F_x = C\cos(\theta) - N\sin(\theta) - f_d\cos(\alpha) + f_l\sin(\alpha) \quad (4)$$

$$F_y = C\sin(\theta) + N\cos(\theta) - f_d\sin(\alpha) - f_l\cos(\alpha) \quad (5)$$

$$M_z = -Ca\sin(\theta) - Na\cos(\theta) + M + m_h \quad (6)$$

where a is the distance from the magnetic clamping point to the center of buoyancy, C is the chord force, N is the normal force, and M is the moment. The variable m_h describes the moment resulting from hydrodynamic dampening as described in [40], f_d is the form drag, and f_l is the lift, and they are given by

$$m_h = \frac{1}{2}\rho\bar{V}^2 A_c\ell\left[\frac{\ell}{\bar{V}}C_{Mw}w + C_{M\alpha}\alpha\right] \quad (7)$$

$$f_d = \frac{1}{2}\rho\bar{V}^2 A_c C_d^b \quad (8)$$

$$f_l = \frac{1}{2}\rho\bar{V}^2 A_c C_l^b \alpha \quad (9)$$

where ρ is the mass density of the water, ℓ is the body length, and A_c is the cross-sectional reference area of the robot platform. The coefficients C_d^b, C_l^b, $C_{M\alpha}$, and C_{Mw} are dimensionless and are a function of the Reynolds number $Re = \rho\ell|V|/\mu$ and the angle of attack α. These coefficients, which are largely geometry dependant, also contain functions that represent modeling uncertainties relating to viscous drag and lift.

C. Flapping IPMC Tail Fin Dynamics

A model has been developed that illustrates the hydrodynamics of an oscillating rigid fin in [41]. The model is found to match experimentally measured forces quite well, and thus it is adapted here and combined with the model expressed in Section III-B. The IPMC actuator and rigid caudal fin are assumed to be sufficiently stiff to minimize cambering and as such can be represented by an oscillating plate. The free body diagram of the oscillating tail is shown in Fig. 5(b), and the movement of the fin can then be described by

$$\theta = \theta_{\max}\sin(\omega t) \quad (10)$$

where ω is the angular frequency of oscillations in radians per second. A velocity vector U_f of the caudal fin can then be defined whose magnitude is given by

$$U_f = \sqrt{r^2\dot{\theta}^2 + \bar{V}^2} \quad (11)$$

where r is the distance from the mounting point of the IPMC to the quarter chord point of the caudal fin and $\bar{V}$ is the velocity of the robot as defined in Section III-B. The angle of attack can then be expressed as

$$\phi = \arctan\left(\frac{r\dot{\theta}\cos\theta - \bar{V}\sin\alpha}{r\dot{\theta}\sin\theta + \bar{V}\cos\alpha}\right). \quad (12)$$

The forces acting on the oscillating fin again are the result of drag, lift, and added mass effects. The forces are expressed in the body's Cartesian coordinate system x, y, and z, defined earlier and centered about the center of buoyancy of the robot. The chord force C (the force axial to the fin) and the normal force N presented in (4)–(6) now become

$$N = N_d + N_l + N_{am} \tag{13}$$

$$C = C_d + C_l + C_{am} \tag{14}$$

where the subscripts d, l, and am denote components of the drag, lift, and added mass effect forces, respectively, normal and axial to the fin.

The dimensionless coefficients C_d^f and C_l^f represent the drag and lift coefficients of the oscillating fin, and are dependant on the operating Reynolds number and the fin geometry. These coefficients are featured in the following equations expressing the lift and drag force components. The components N_d, C_d, N_l, and C_l can then be written as:

$$N_d = \frac{1}{2} C_d^f \rho A_f U_f^2 \sin(\phi + \theta) \tag{15}$$

$$C_d = -\frac{1}{2} C_d^f \rho A_f U_f^2 \cos(\phi + \theta) \tag{16}$$

$$N_l = \frac{1}{2} C_l^f \sin\phi \rho A_f U_f^2 \cos(\phi + \theta) \tag{17}$$

$$C_l = \frac{1}{2} C_l^f \sin\phi \rho A_f U_f^2 \sin(\phi + \theta) \tag{18}$$

with A_f being the projected fin area normal to U_f.

The added mass coefficients for a 2-D thin plate derived in [42] are $\mu_c = 0$, $\mu_n = \rho\pi b^2$, $\mu_{nc} = 0$, $\mu_{cw} = 0$, $\mu_{nw} = \rho\pi b^3$, and $\mu_w = (9/8)\rho\pi b^4$. Here, b is half the length of the fin. The force components are then

$$N_{am} = h \left[-\mu_{nc}\dot{U}_c - \mu_n \dot{U}_n - \mu_{nw}\ddot{\theta} \right.$$
$$\left. -\dot{\theta}(\mu_c U_c + \mu_{nc} U_n + \mu_{cw}\dot{\theta}) \right] \tag{19}$$

$$C_{am} = h \left[-\mu_c \dot{U}_c - \mu_{nc}\dot{U}_n - \mu_{cw}\ddot{\theta} \right.$$
$$\left. +\dot{\theta}(\mu_{nc} U_c + \mu_n U_n + \mu_{nw}\dot{\theta}) \right] \tag{20}$$

where h is the fin width (in the z-direction), and U_n and U_c are the components of U_f normal and axial to the fin, respectively, and are given by

$$U_n = -U_f \sin(\phi + \theta) \tag{21}$$

$$U_c = U_f \cos(\phi + \theta). \tag{22}$$

The moment M generated by the flapping caudal fin is given by [42]

$$M = -h \left[\mu_{cw}\dot{U}_c + \mu_{nw}\dot{U}_n + \mu_w\ddot{\theta} + \mu_{nc}\left(U_c^2 - U_n^2\right) \right.$$
$$\left. + (\mu_n - \mu_c)U_c U_n + (\mu_{nw}U_c - \mu_{cw}U_n)\dot{\theta} \right]. \tag{23}$$

IV. CHARACTERIZATION

IPMC actuators demonstrate significant aptitude for producing smooth complex motion that is largely unrealized
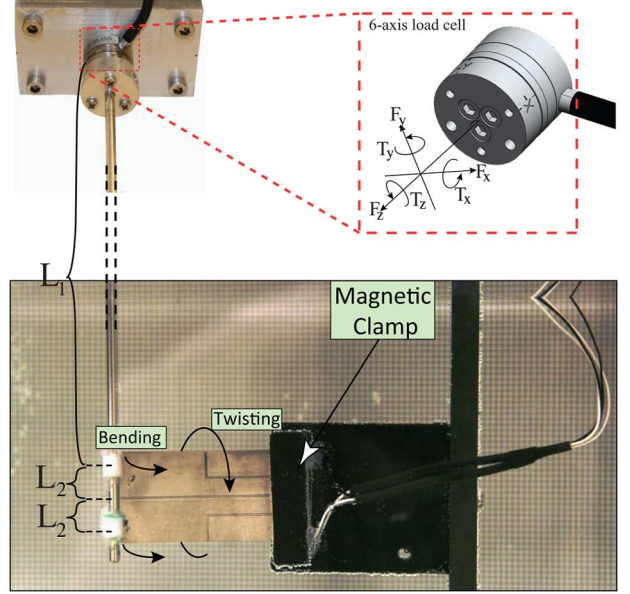

Fig. 6. Experimental setup for measuring the propulsor's blocking force and torque. The IPMC-caudal fin is actuated in water and fixed to a load cell.

by conventional actuation techniques [43]. However, understanding the capabilities of IPMCs with respect to blocking force and torque, and bending and twisting response is essential to successful development of practical robotic systems. Also, the knowledge of the operational characteristics of the actuator can be used to validate and improve models. In this section, the performance of both conventional and sectored IPMCs is characterized.

The experimental setup using two laser displacement sensors [Micro-Epsilon (Ortenburg, Germany), optoNCDT 1401] to measure twisting performance is shown in Fig. 1(a). A custom-design National Instruments (Austin, TX, USA) LabVIEW program is used to generate and output the actuation signal and monitor the sensor's response (related to IPMC range of motion and generated loads). A six-axis load cell [ATI Industrial Automation (Apex, NC, USA) Nano17-Ti, with resolution down to 0.149 mN of linear force and 0.0069-N·mm torque] is used to measure loads of interest. The load cell's coordinate system as well as the experimental setup, in which a magnetic clamp is used to hold the IPMC in the desired location and provide electrical power, are shown in Fig. 6. A 3.18-mm (1/8-in) diameter rod made of 304 stainless steel is used for mechanical amplification of tip force. The measured torque about the x-axis (T_x in Fig. 6) is used to resolve the blocking force and the blocking torque.

A. Twisting Response

It is necessary for IPMCs to bend and twist to realize propulsive movements that would be beneficial to any underwater vehicle or platform. Without patterned electrodes, a conventional IPMC actuator is not capable of generating twisting motion. However, utilizing a flexible medium in conjunction with multiple IPMCs to create a structure that can generate twisting and complex deformation is a feasible alternative [26]. For example, see the robotic system in Fig. 15(a). For
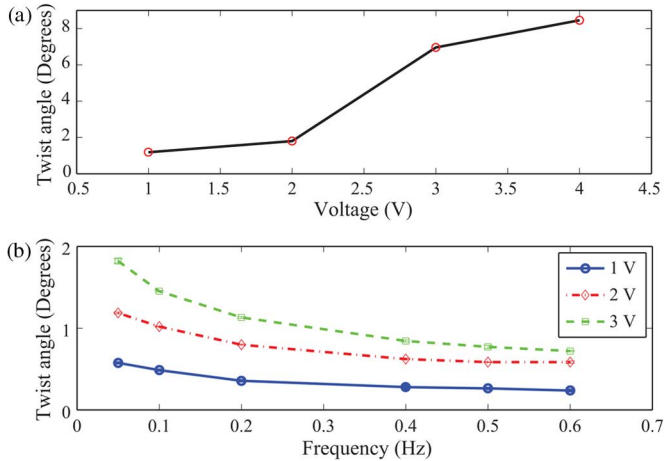
Fig. 7. (a) Twist angle of IPMC versus amplitude of dc input voltage and (b) twist angle versus input signal frequency (sinusoidal input).

Fig. 8. Blocking force of sectored IPMC versus input signal frequency.

Fig. 9. Blocking torque of sectored IPMC versus input signal frequency.

the monolithic IPMC with four separate electrode pads [see Fig. 1(b)], twisting motion is generated by phase shifting the input signal of the left and right sectors (e.g., by 180°) relative to each other. In the case of 180° phase shifting, the patterned IPMC can achieve a maximum twist angle of 8.46° under a 4-V dc input. Furthermore, it was found that the twist angle increases dramatically with increasing input voltages as well as decreasing actuation frequency (sinusoidal input). These trends are found in Fig. 7(a) and (b), showing the ability to produce practical twisting motion.

B. Blocking Force and Torque

Bending and twisting movements illustrate the potential use of IPMCs as both control surfaces and tools for active maneuvering. However, any control or maneuvering forces generated are ultimately limited by the blocking strength of the actuator. The blocking force and torque are defined here as the maximum tip force or torque that can be generated by the actuator with zero deflection (displacement).

In [44], tip force, referenced as generative force (F_T), was found to increase with applied voltage, decrease with tip deflection, and display a cubic relationship with membrane thickness that can be explained by Hooke's law. The tip force again was characterized for surface resistance and effective bending length parameters in [33]. Herein, the blocking force and the blocking torque are experimentally obtained for the sectored IPMC seen in Fig. 1(b).

To measure blocking force, sinusoidal voltage inputs with amplitudes of 1, 2, and 3 V were applied to the IPMC at frequencies ranging from 0.05 to 2 Hz, with each pad receiving the same input. For blocking torque measurements, inputs on the same frequency range with amplitudes of 2, 3, and 4 V were applied, with a phase shift of 180° between the left and right electrode pairs. The results for blocking force and blocking torque are presented in Figs. 8 and 9, respectively. Both blocking strength characteristics are found to increase with decreasing input frequency. However, two separate growth regimes are observed on either side of a threshold of about 0.2 Hz. At frequencies greater than 0.2 Hz, the blocking force and torque exhibit quasi-linear
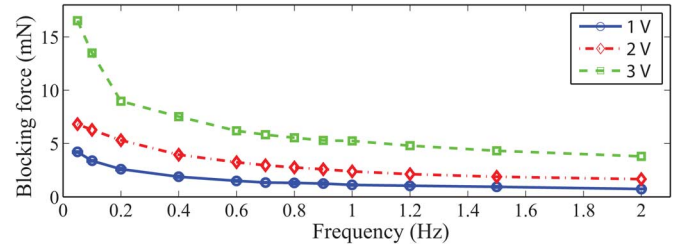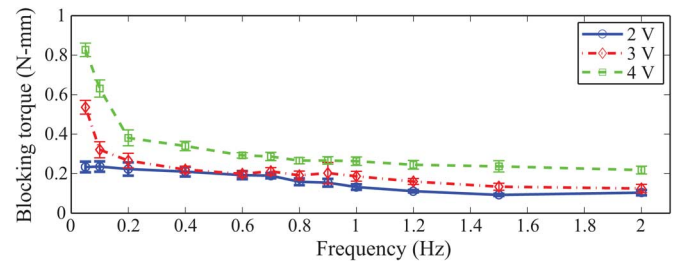
growth with decreased frequency while, at frequencies less than 0.2 Hz, there is a rapid increase of these loads. This behavior can be attributed to the fact that the transient response of mobile cations induces stress, and in effect tip force and torque. The maximum blocking force measured is 16.5 mN at 3 V and the maximum blocking torque is 0.83 N · mm at 4 V (for IPMC sample shown in Fig. 1), both occurring at the minimum input frequency of 0.05 Hz.

C. Propulsion Characteristics

Existing underwater propulsion systems for underwater robotic platforms are currently dominated by conventional propeller designs. On the contrary, bioinspired designs are still in the infant stage. With respect to underwater locomotion, substantial improvements can be made in the areas of efficiency and maneuverability by mimicking biological forms of locomotion [2]. IPMCs can be exploited to replicate smooth motions seen in nature. Typical propulsion techniques employed by aquatic animals, particularly fish, feature flexible foils in combination with motions such as flapping, heaving, or both. The tail, or caudal fin, is the primary propulsor for most of these animals. In this section, an IPMC in conjunction with a passive tail element (caudal fin) is tested for its ability to generate thrust.

With this in mind, a conventional IPMC sample connected to a trapezoidal caudal fin [Fig. 10(a)] was tested to verify the ability to extrapolate thrust force from the experimental setup. The fin was secured to the IPMC with Kapton polyimide film tape. Kapton tape was chosen for its silicone adhesive that is more water resistant than conventional acrylic or rubber adhesive tapes. A nylon block featuring neodymium magnet clamps was installed at the end of the stainless steel rod while the rod itself was secured to the load cell via a set screw. The IPMC-caudal fin assembly was secured in the magnetic clamps and actuated in water. The experimental setup with the load cell is illustrated in Fig. 10. The thrust force was then backed out from the torque measured about the load cell's x-axis by $T_x = F_T \cdot L$.
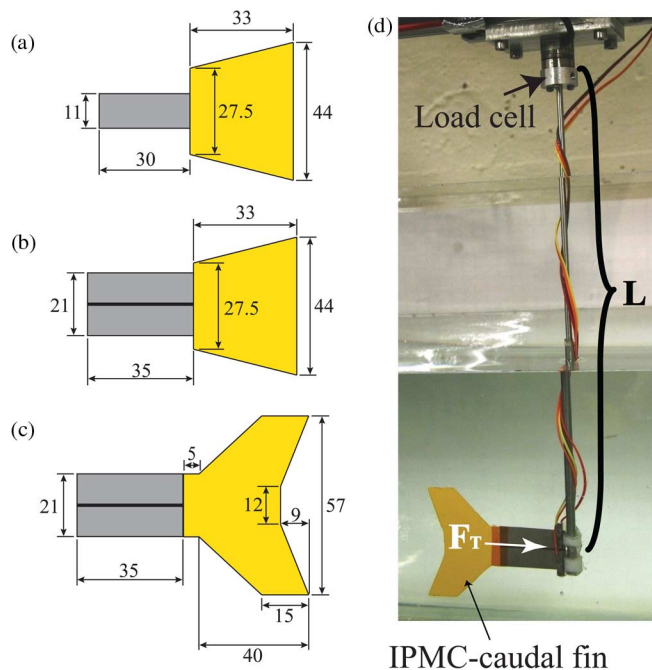
Fig. 10. IPMC-caudal fin assemblies used for thrust testing (units in mm): (a) conventional IPMC sample with simple trapezoidal caudal fin, sectored IPMC (b) with simple caudal fin, and (c) with bioinspired caudal fin. (d) Experimental setup for characterizing the propulsor's thrust capabilities.
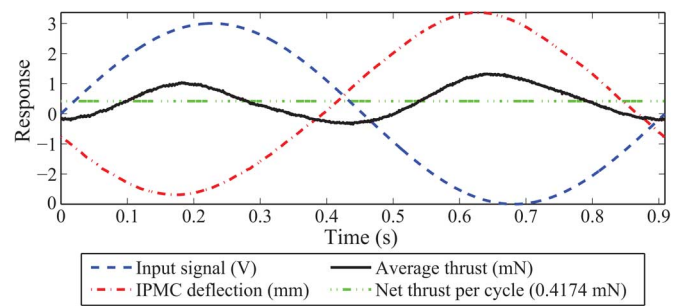

Fig. 11. Thrust response of conventional IPMC with caudal fin when driven by a 3-V, 1.1-Hz sine wave (operating at resonance).
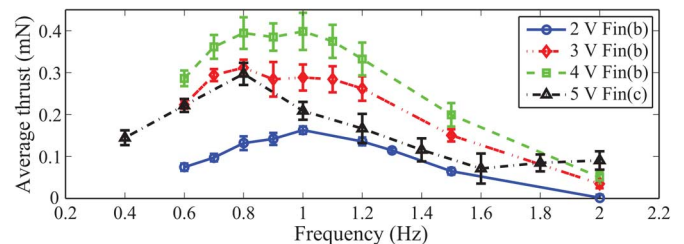

Fig. 12. Thrust production of sectored IPMC in conjunction with caudal fin shapes shown in Fig. 10(b) and (c) when actuated by sinusoidal input voltages.

The frequency response measured between the applied input voltage and resulting bending displacement of the IPMC-caudal fin assembly revealed a dominant resonance at 1.1 Hz. Fig. 11 shows the thrust and displacement profiles for the IPMC when actuated at resonance. The per-cycle thrust measurement profile is compared to experimental results obtained in [17] and [45], numerical simulation analyses performed in [46] and [37], and predicted results from models in [47] and [48]. The behavior correlates, based on two observations: 1) the frequency of the thrust is twice that of the IPMC actuation frequency; and 2) essentially zero thrust is observed when there is zero deflection. Additionally, two other behaviors are also consistent with the expected system behavior. First, the peak thrust points occur very near inflection points of the IPMC deflection, which is to be expected given the thrust's dependence on both θ and the velocity of the fin. Second, one would expect a 180° phase lag between the input signal and the IPMC deflection at resonance. By inspection of Fig. 11, a phase lag of nearly 180° is observed.

Thrust force was experimentally measured for a sectored IPMC with two different caudal fin geometries. A conventional IPMC sample with dimensions of 21 mm × 35 mm was bisectored to create one IPMC consisting of two separate 10 mm × 35 mm electrode pads. A passive caudal fin was attached and used to aid in thrust production as preliminary testing indicated that thrust generated by the rectangular-shaped IPMC itself is relatively smaller than when coupled with a rigid fin. Lexan plastic 50 μm thick was chosen as the fin material for its high stiffness-to-weight ratio. The fin geometries used, a simple trapezoidal caudal fin and a bioinspired fin approximately 11.8% larger, are shown in Fig. 10(b) and (c), respectively.

The caudal fins were actuated over frequencies ranging from 0.1 to 2 Hz for the trapezoidal shape and 0.4–2.6 Hz for the bioinspired geometry. The measured thrust was then averaged over a minimum of eight cycles. The resulting average thrust values are reported in Fig. 12.

Using the trapezoidal fin over the given range, a maximum average thrust of 0.4 mN was observed, with an input of 4 V at 1 Hz. When the biomimetic caudal fin is used, a maximum thrust of 0.3 mN was found with an input of 5 V and an actuation frequency of 0.8 Hz. This peak value occurs at a lower frequency than in the case of a trapezoidal caudal fin. Interestingly, despite the bioinspired caudal fin's larger surface area, thrust forces are approximately 26% lower at a 25% higher actuation voltage. This can be attributed to hydrodynamic effects relating to the complex geometry; particularly the cutout on the trailing edge and its effect on vortex production. Experimental results show that thrust generation is heavily dependent on actuation frequency, as well as the configuration of the IPMC and caudal fin geometry.

D. Power Consumption and Effectiveness

The power consumption of IPMC actuators is dependant on several factors, the first of which is the size or geometry of the actuator itself. The mechanism behind IPMC actuation is the migration of mobile cations in response to transient charge behavior on the IPMC's surface. Increasing the size of the actuator results in more mobile cations and increased charge dynamics, which contributes to increased power consumption. Second, when applied potentials become too large, an electrolytic process known as electrolysis can occur. The standard potential of the water electrolysis cell at 25 °C is 1.23 V at a pH of 7, but in the case of IPMCs, it may be higher, depending on experimental conditions and material properties. In [49], the electrolysis point for an IPMC was found to be 1.8 V. Past this point, the resulting reduction reaction splits water into hydrogen and oxygen, resulting in a higher current draw than
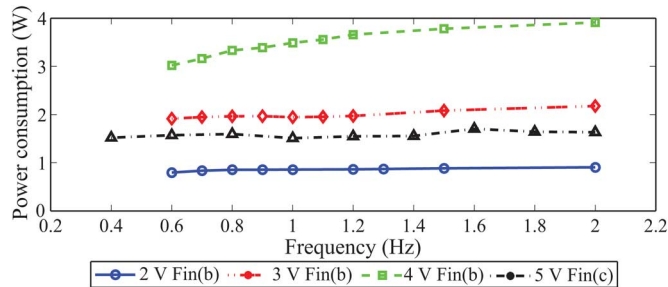
Fig. 13. Power consumption of sectored IPMC and caudal fins seen in Fig. 10(b) and (c) when actuated by sinusoidal input voltages.

Fig. 14. The ratio of average thrust force to power consumed, Υ, for sectored IPMC and caudal fins from Fig. 10(b) and (c) versus frequency of sinusoidal input voltage.

is necessary for IPMC actuation. The energy consumed in this process does not aid in thrust production and results in large inefficiencies. The degree to which electrolysis occurs in the actuation cycle is determined by the magnitude of the applied voltage (e.g., electrolysis happens more readily at 5 V than at 3 V) and the shape or dynamic properties of the input waveform.

The power consumption was determined by calculating instantaneous power consumption over a minimum of eight actuation cycles and then taking the mean over the course of the cycle. The resulting power consumption for the sectored IPMC-caudal fin assemblies is shown in Fig. 13. As the applied voltage increases, the power consumption increases nonlinearly for the trapezoidal caudal fin. However, this trend stops when the bioinspired caudal fin is examined. This fin consumes less than half the power of the trapezoidal fin despite being actuated at a 25% higher applied voltage.

To quantify the effectiveness of the propulsor, the ratio of thrust force to power consumption, defined as Υ, is introduced

$$\Upsilon = \frac{T_{\text{ave}}}{P} \qquad (24)$$

where T_{ave} is the average thrust per actuation cycle, P is the corresponding power consumption, and Υ has the units mN/W. This ratio is plotted for all cases in Fig. 14. When examining the three amplitudes of the sinusoidal input voltages for the trapezoidal fin, it can be seen that increasing the voltage to generate more thrust is a game of diminishing returns. Any increase in thrust gained from an increased input voltage results in a disproportionate increase in power consumption. Interestingly, in the case of the bioinspired fin, the Υ value of the fin is on par with the value of a trapezoidal fin at 2 V, despite its drastically higher operating voltage of 5 V. It is suspected that the geometry of the bioinspired caudal fin minimizes drag perpendicular to the fin and thus reduces energy consumption throughout the cycle. Complex fluid interactions related to vortex generation are also likely involved. Further experimentation will need to be conducted to draw concrete conclusions.

V. PERFORMANCE OF ROBOTIC FISH

A. Robotic Platforms

Two robotic systems were created to demonstrate the application of the IPMCs, as shown in Fig. 15. The first platform is controlled by platinum and gold IPMCs (see Section II-B for gold plating process). The pectoral fins consist of four IPMCs (two per side) with one actuator at the leading and trailing edge
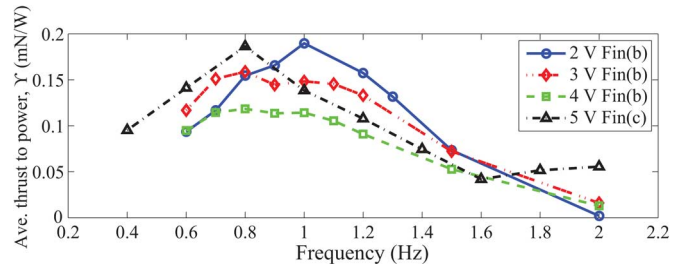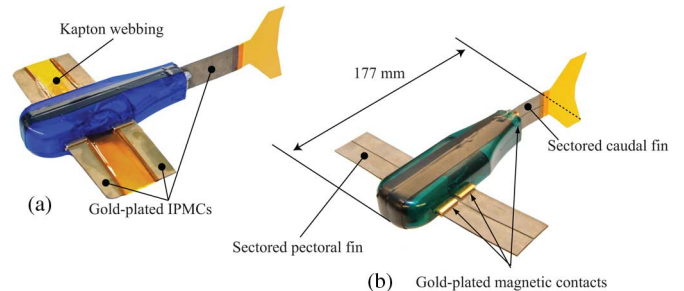

Fig. 15. Two bioinspired IPMC-based robots: (a) platform with gold-plated IPMCs with pectoral fins consisting of individual actuators connected by Kapton film and (b) platform with three bisectored IPMCs.

of each pectoral fin. As previously mentioned, if the electrodes of the IPMC are not patterned, this is an alternative approach to generate twisting motion. Specifically, the two IPMCs are connected by a webbing of Kapton film. The purpose of this webbing is to provide a control surface that reflects the movement of the IPMCs and to generate a twisting motion when the IPMCs are not actuated in unison. The caudal fin is made of a conventional IPMC with a rigid (passive) tail fin [design Fig. 10(c)] for enhanced thrust capabilities.

For the second design, three monolithic IPMCs featuring a bisectored pattern are used as the right and left pectoral fins and as a tail assembly featuring a rigid caudal fin [Fig. 10(c)]. Up to this point, biorobotic fish have used the caudal fin both for propulsion and maneuverability by way of changing the duty cycle or biasing the input voltage so that the caudal fin does not oscillate about a neutral axis [16], [36]. This allows the robot motion in the yaw plane. By utilizing sectored IPMCs as pectoral fins, more degrees of freedom can be achieved, and, thus, more complex maneuvering is realized. For example, by propelling the robot forward and then twisting the pectoral fins in opposite directions, the robot body can roll. Then, twisting the pectoral fins in the same direction would result in a banking motion of the entire robot.

A modular robot body with a mechanism for quick and easy removal of the fins was created using gold plated magnets as the contact and power delivery mechanisms. This design allows quick modification of fin configuration and geometry. Slots were machined into the acrylic body to accommodate the gold plated magnetic clips. The robot was partially filled with silicone casting rubber to tailor its buoyancy. For simplicity, the robots are tethered to an external power source for testing. This modular design allows for an easy exchange of pectoral and
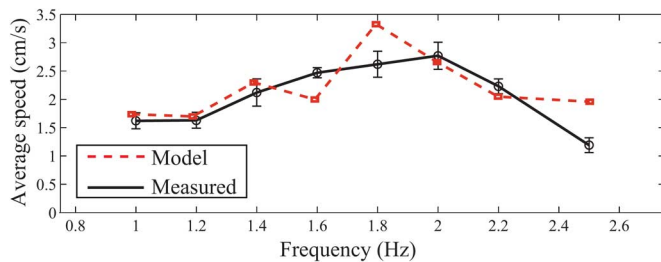
Fig. 16. Experimentally measured swimming speed of the robotic system compared to model's prediction when actuated by 5-V sinusoidal input.

caudal fin assemblies as well as repair of electrical contacts. If a wireless design was developed, the electronics package could fit inside the body cavity without further modification. The finished platform has a mass of 67.4 g and is 177 mm long [see Fig. 15(b)].

B. Performance

The platform's caudal fin was actuated with a sine wave with a 5-V amplitude over a range of frequencies (three runs at each frequency), while the robot's motion was recorded with a video camera from two angles with a 1-cm grid in the background. The video was then analyzed to obtain an average speed, resulting in six measurements for each frequency. The average speed of the robot as a function of the actuation frequency can be seen in Fig. 16. The maximum average speed (2.8 cm/s or 0.16 body-lengths/s) is found at an actuation frequency of 2 Hz, making the effective Reynolds number approximately 4890. Intuitively, one would expect that the maximum speed of the robot would correspond to the frequency at maximum thrust, as presented in Fig. 12. However, it is found that this is not the case, because, at low actuation frequencies, the large tail actuation amplitude results in large yaw angles of the robot body. This has a limiting effect on forward speed. At frequencies greater than 1 Hz, this effect is reduced and reaches an optimum level at 2 Hz, where the maximum speed occurs. A similar conclusion was made for an IPMC enabled robot in [36].

The optimal range of the Strouhal number (St) for efficient swimming modes has been identified to lie between 0.25 and 0.4 [50]. Indirectly, it was shown that fish propulsion occurs where $0.25 < \text{St} < 0.35$ [51]. The Strouhal number of the robotic platform at maximum speed is found to be approximately 0.72. This value being outside the range of optimal swimming efficiency is attributed to the caudal fin being of arbitrary design and its geometry and size not being tuned to the length and width of the IPMC actuator. Significant improvements in swimming speed can be made, for example, by optimizing the IPMC-caudal fin geometry.

VI. CONCLUSION

The ability of sectored IPMCs to realize bending and twisting motion was experimentally quantified. Thrust production of a sectored IPMC with a passive caudal fin element was investigated for two different fin geometries. This ability was discussed with respect to power consumption. The ratio of average thrust force to power consumed, Υ, was defined to reflect the effectiveness of a tail fin. This information was used to develop a bioinspired robotic system capable of ostraciiform locomotion with potential to control pitch, roll, and yaw through complex twisting of the pectoral and tail fins. The maximum speed for the initial platform was found to be 2.8 cm/s.

Future innovations toward performance improvement of IPMCs in the areas of blocking force and stiffness will improve the attractiveness of incorporating sectored IPMCs for this purpose. These advances will also open up opportunities to generate more complex biomimetic motions such as undulations without needing independent flexible media. However, utilizing simple surface machining techniques to produce patterned IPMCs capable of complex deformation is a reality, and the potential to use these surfaces to actively control underwater robotic systems capable of multiple degrees of freedom is possible.

REFERENCES

[1] P. R. Bandyopadhyay, D. N. Beal, and A. Menozzi, "Biorobotic insights into how animals swim," *J. Exp. Biol.*, vol. 211, pp. 206–214, 2008.

[2] P. R. Bandyopadhyay, "Maneuvering hydrodynamics of fish and small underwater vehicles," *Integr. Compar. Biol.*, vol. 42, no. 1, pp. 102–117, 2002.

[3] D. R. Yoerger, J. G. Cooke, and J. J. Slotine, "The influence of thruster dynamics on underwater vehicle behavior and their incorporation into control system design," *IEEE J. Ocean. Eng.*, vol. 15, no. 3, pp. 167–178, Jul. 1990.

[4] M. Shahinpoor, Y. Bar-Cohen, J. O. Simpson, and J. Smith, "Ionic polymer-metal composites (IPMCs) as biomimetic sensors, actuators and artificial muscles-a review," *Smart Mater. Struct.*, vol. 7, no. 6, pp. R15–R30, 1998.

[5] K. J. Kim and M. Shahinpoor, "Ionic polymer-metal composites: II. Manufacturing techniques," *Smart Mater. Struct.*, vol. 12, no. 1, pp. 65–79, 2003.

[6] M. Shahinpoor and K. J. Kim, "Ionic polymer-metal composites: IV. industrial and medical applications," *Smart Mater. Struct.*, vol. 14, no. 1, pp. 197–214, 2005.

[7] M. Shahinpoor, "Conceptual design, kinematics and dynamics of swimming robotic structures using ionic polymeric gel muscles," *Smart Mater. Struct.*, vol. 1, no. 1, pp. 91–94, 1992.

[8] D. Pugal, K. Jung, A. Aabloo, and K. J. Kim, "Ionic polymermetal composite mechanoelectrical transduction: Review and perspectives," *Polymer Int.*, vol. 59, no. 3, pp. 279–289, 2010.

[9] G. Alici, G. M. Spinks, J. D. Madden, Y. Wu, and G. G. Wallace, "Response characterization of electroactive polymers as mechanical sensors," *IEEE/ASME Trans. Mechatron.*, vol. 13, no. 2, pp. 187–196, Apr. 2008.

[10] K. Kruusamae, P. Brunetto, S. Graziani, A. Punning, G. Di Pasquale, and A. Aabloo, "Self-sensing ionic polymer-metal composite actuating device with patterned surface electrodes," *Polymer Int.*, vol. 59, no. 3, pp. 300–304, 2010.

[11] E. Smela, M. Kallenbach, and J. Holdenried, "Electrochemically driven polypyrrole bilayers for moving and positioning bulk micromachined silicon plates," *J. Microelectromech. Syst.*, vol. 8, no. 4, pp. 373–383, Dec. 1999.

[12] Y. Nakabo, T. Mukai, and K. Asaka, "Kinematic modeling and visual sensing of multi-DOF robot manipulator with patterned artificial muscle," in *Proc. IEEE Int. Conf. Robot. Autom.*, Barcelona, Spain, 2005, pp. 4315–4320.

[13] J. H. Jeon, S.-W. Yeom, and I.-K. Oh, "Fabrication and actuation of ionic polymer metal composites patterned by combining electroplating with electroless plating," *Composites A*, vol. 39, no. 4, pp. 588–596, 2008.

[14] M. Fleming, K. J. Kim, and K. K. Leang, "Mitigating IPMC back relaxation through feedforward and feedback control of patterned electrodes," *Smart Mater. Struct.*, vol. 21, no. 8, 2013, DOI: 10.1088/0964-1726/21/8/085002.

[15] K. J. Kim, D. Pugal, and K. K. Leang, "A twistable ionic polymer-metal composite artificial muscle for marine applications," *Mar. Technol. Soc. J.*, vol. 45, no. 4, pp. 83–98, 2011.

[16] B. Kim, D.-H. Kim, J. J. Jung, and J.-O. Park, "A biomimetic undulatory tadpole robot using ionic polymer-metal composite actuators," *Smart Mater. Struct.*, vol. 14, pp. 1579–1585, 2005.

[17] M. Aureli, V. Kopman, and M. Porfiri, "Free-locomotion of underwater vehicles actuated by ionic polymer metal composites," *IEEE/ASME Trans. Mechatron.*, vol. 15, no. 4, pp. 603–614, Aug. 2010.

[18] S. Guo, Y. Ge, L. Li, and S. Liu, "Underwater swimming micro robot using IPMC actuator," in *Proc. IEEE Int. Conf. Mechatron. Autom.*, Luoyang, China, Jun. 25–28, 2006, pp. 249–254.

[19] X. Ye, Y. Su, and S. Guo, "A centimeter-scale autonomous robotic fish actuated by IPMC actuator," in *Proc. IEEE Int. Conf. Robot. Biomimetics*, 2007, pp. 262–267.

[20] S. Xu, B. Liu, and L. Hao, "A small remote operated robotic fish actuated by IPMC," in *Proc. IEEE Int. Conf. Robot. Biomimetics*, 2008, pp. 1152–1156.

[21] X. Tan, D. Kim, N. Usher, D. Laboy, J. Jackson, A. Kapetanovic, J. Rapai, B. Sabadus, and X. Zhou, "An autonomous robotic fish for mobile sensing," in *Proc. IEEE/RSJ Int. Conf. Intell. Robots Syst.*, Beijing, China, 2006, pp. 5424–5429.

[22] G. Chamorro, "Swimming robotic structures equipped with IPMC artificial muscles," M.S. thesis, Dept. Mech. Eng., Univ. New Mexico, Albuquerque, NM, USA, 2000.

[23] M. Mojarrad, "Study of ionic polymeric gels as smart materials and artificial muscles for biomimetic swimming robotic applications," Ph.D. dissertation, Dept. Mech. Eng., Univ. New Mexico, Albuquerque, NM, USA, 2001.

[24] Z. Chen, S. Shatara, and X. Tan, "Modeling of biomimetic robotic fish propelled by an ionic polymer-metal composite caudal fin," *IEEE/ASME Trans. Mechatron.*, vol. 15, no. 3, pp. 448–459, Jun. 2010.

[25] S. Yeom and I. I. Oh, "Fabrication and evaluation of biomimetic jellyfish robot using IPMC," in *Proc. 3rd Int. Conf. Smart Mater. Struct. Syst.*, 2008, vol. 58, pp. 171–176.

[26] Z. Chen, T. Um, and H. Bart-Smith, "A novel fabrication of ionic polymer-metal composite membrane actuator capable of 3-dimensional kinematic motions," *Sens. Actuators A, Phys.*, vol. 168, no. 1, pp. 131–139, 2011.

[27] Z. Chen, T. I. Um, and H. Bart-Smith, "Bio-inspired robotic manta ray powered by ionic polymer-metal composite artificial muscles," *Int. J. Smart Nano Mater.*, vol. 3, no. 4, pp. 296–308, 2012.

[28] M. Yamakita, N. Kamamichi, T. Kozuki, K. Asaka, and Z. W. Luo, "A snake-like swimming robot using IPMC actuator and verification of doping effect," in *Proc. IEEE/RSJ Int. Conf. Intell. Robots Syst.*, 2005, pp. 2035–2040.

[29] K. Abdelnour, A. Stinchcombe, M. Porfiri, J. Zhang, and S. Childress, "Wireless powering of ionic polymer metal composites toward hovering microswimmers," *IEEE/ASME Trans. Mechatron.*, vol. 17, no. 5, pp. 924–935, Oct. 2012.

[30] S. Guo, L. Shi, and K. Asaka, "IPMC actuator-based an underwater microrobot with 8 legs," in *Proc. IEEE Int. Conf. Mechatron. Autom.*, 2008, pp. 551–556.

[31] K. Takagi, M. Yamamura, Z. W. Luo, M. Onishi, S. Hirano, K. Asaka, and Y. Hayakawa, "Development of a Rajiform swimming robot using ionic polymer artificial muscles," in *Proc. IEEE/RSJ Int. Conf. Intell. Robots Syst.*, 2006, pp. 1861–1866.

[32] J. Hubbard, M. Fleming, K. K. Leang, V. Palmre, D. Pugal, and K. J. Kim, "Characterization of sectored-electrode IPMC-based propulsors for underwater locomotion," in *Proc. ASME Conf. Smart Mater. Adaptive Struct. Intell. Syst.*, Scottsdale, AZ, USA, 2011, pp. 171–180.

[33] S. G. Lee, H. Park, S. D. Pandita, and Y. Yoo, "Performance improvement of IPMC (ionic polymer metal composites) for a flapping actuator," *J. Control Autom. Syst.*, vol. 4, no. 6, pp. 748–755, 2006.

[34] M. Aureli, V. Kopman, and M. Porfiri, "Control-oriented modeling of ionic polymer metal composites for biomimetic underwater propulsion," in *Proc. Amer. Control Conf.*, 2010, pp. 6016–6021.

[35] N. N. Pak and S. Scapellato, "Biomimetic design of a polychaete robot using IPMC actuator," in *Proc. Int. Conf. Biomed. Robot. Biomechatron.*, 2006, pp. 666–671.

[36] S. McGovern, G. Alici, V. Truong, and G. Spinks, "Finding NEMO (novel electromaterial muscle oscillator): A polypyrrole powered robotic fish with real-time wireless speed and directional control," *Smart Mater. Struct.*, vol. 18, 2009, DOI: 10.1088/0964-1726/18/9/095009.

[37] M. Bozkurttas, J. Tangorra, G. Lauder, and R. Mittal, "Understanding the hydrodynamics of swimming: From fish fins to flexible propulsors for autonomous underwater vehicles," *Adv. Sci. Technol.*, vol. 58, pp. 193–202, 2008.

[38] M. Sfakiotakis, D. M. Lane, and J. B. Davies, "Review of fish swimming modes for aquatic locomotion," *IEEE J. Ocean. Eng.*, vol. 24, no. 2, pp. 237–252, Apr. 1999.

[39] T. I. Fossen, *Guidance and Control of Ocean Vehicles*, 1 ed. New York, NY, USA: Wiley, 1994.

[40] V. Stepanyan, N. Hovakimyan, and C. A. Woolsey, "Adaptive output feedback control of a spheroidal underactuated underwater vehicle," in *Proc. MTS/IEEE OCEANS Conf.*, vol. 1, pp. 278–284.

[41] P. Kodati, J. Hinkle, A. Winn, and D. Xinyan, "Microautonomous robotic ostraciiform (marco): Hydrodynamics, design, and fabrication," *IEEE Trans. Robot.*, vol. 24, no. 1, pp. 105–117, Feb. 2008.

[42] L. I. Sedov, *Two-Dimensional Problems in Hydrodynamics and Aerodynamics*. New York, NY, USA: Interscience Publishers, 1965.

[43] J. D. W. Madden, N. A. Vandesteeg, P. A. Anquetil, P. G. A. Madden, and A. Takshi, "Artificial muscle technology: Physical principles and naval prospects," *IEEE J. Ocean. Eng.*, vol. 29, no. 3, pp. 706–728, Jul. 2004.

[44] K. J. Kim and M. Shahinpoor, "A novel method of manufacturing three-dimensional ionic polymer-metal composites (IPMCs) biomimetic sensors, actuators and artificial muscles," *Polymer*, vol. 43, no. 3, pp. 797–802, 2002.

[45] S. McGovern, M. Abbot, R. Emery, and G. Alici, "Evaluation of thrust force generated for a robotic fish propelled with polypyrrole actuators," *Polymer Int.*, vol. 59, pp. 357–364, 2010.

[46] I. Akhtar, R. Mittal, G. V. Lauder, and E. Drucker, "Hydrodynamics of a biologically inspired tandem flapping foil configuration," *Theor. Comput. Fluid Dyn.*, vol. 21, pp. 155–170, 2007.

[47] K. A. Harper, M. D. Berkemeier, and S. Grace, "Modeling the dynamics of spring-driven oscillating-foil propulsion," *IEEE J. Ocean. Eng.*, vol. 23, no. 3, pp. 285–296, Jul. 1998.

[48] D. Xia, J. Liu, W. Chen, and L. Han, "Hydrodynamic analysis of fish-like robot swimming in the straight forward way," in *Proc. IEEE Int. Conf. Mechatron. Autom.*, 2009, pp. 3342–3347.

[49] D. Kim and K. J. Kim, "Experimental investigation on electrochemical properties of ionic polymer-metal composite," *J. Intell. Mater. Syst. Struct.*, vol. 17, no. 5, pp. 449–454, 2006.

[50] M. S. Triantafyllou and G. S. Triantafyllou, "An efficient swimming machine," *Sci. Amer.*, vol. 272, pp. 64–71, 1995.

[51] P. R. Bandyopadhyay, "Maneuvering hydrodynamics of fish and small underwater vehicles," *Integr. Comput. Biol.*, vol. 42, pp. 102–117, 2002.

Joel J. Hubbard received the B.S. and M.S. degrees in mechanical engineering from the University of Nevada—Reno, Reno, NV, USA, in 2009 and 2011, respectively.

Afterwards, he was commissioned as an Ensign and Surface Warfare Officer (Nuclear) in the U.S. Navy. ENS Hubbard is currently serving onboard the Landing Helicopter Dock, the *USS ESSEX (LHD-2)*, as the Assistant Navigator and acting as a Project Manager during its $200 million Extended Dry-Docked Phased Maintenance Availability.

Maxwell Fleming received the B.S. and M.S. degrees in mechanical engineering from the University of Nevada—Reno, Reno, NV, USA, in 2010 and 2012, respectively.

His research focused on modeling and control of ionic polymer–metal composites (IPMCs). He is currently working as an Engineer at Novartis Consumer Health, Inc., Waverly, NE, USA.

Viljar Palmre received the B.S., M.S., and Ph.D. degrees in materials science from the University of Tartu, Tartu, Estonia, in 2006, 2008, and 2012, respectively. He is currently working toward the Ph.D. degree in materials science and engineering at the University of Nevada—Reno, Reno, NV, USA.

His research interests are electroactive polymers with a focus on synthesis and design of ionic polymer–metal composites.

David Pugal received the M.S. degree in applied physics from the University of Tartu, Tartu, Estonia, in 2008 and the Ph.D. degree in mechanical engineering from the University of Nevada—Reno, Reno, NV, USA, in August 2012.

He has been studying ionic polymer–metal composite (IPMC) materials since 2007 with the focus on developing a physics-based finite element model to describe the transduction of the material. He has also been participating in development of an open source finite element solver Hermes2D to provide an hp-FEM implementation of the underlying equations that describe the bending of IPMCs.

Kwang J. Kim received the Graduate degree from Yonsei University, Seoul, Korea, in 1987 and the M.S. and Ph.D. degrees from Arizona State University (ASU), Phoenix, AZ, USA, in 1989 and 1992, respectively, all in chemical engineering.

He is currently the Southwest Gas Professor of Energy and Matter at the Mechanical Engineering Department, University of Nevada—Las Vegas (UNLV), Las Vegas, NV, USA. Prior to joining UNLV in fall 2012, he was the Foundation Professor and Chair of the Mechanical Engineering Department (2007–2012) at the University of Nevada—Reno (UNR), Reno, NV, USA. He completed a postdoctoral study at the University of Maryland—College Park (UMCP; 1993–1995), College Park, MD, USA. His industrial experience includes Senior Research Engineer at Thermal Electric Devices, Inc. (1995–1997) and Chief Scientist at Environmental Robots, Inc., Albuquerque, NM, USA (1997–2001). His research interests are in a broad spectrum of energy systems and active materials/sensors. He has authored/coauthored more than 300 technical publications including more than 130 refereed journal papers and three monographs and was awarded two U.S. patents.

Dr. Kim is a recipient of the 2011 UNR Foundation Professorship, the 2006 UNR Lemelson Award for Innovation and Entrepreneurship, and the 2002 Ralph E. Powe Junior Faculty Enhancement Award from Oak Ridge Associated Universities. He is a Fellow of the American Society of Mechanical Engineers (ASME) and currently serves on the editorial boards of *Smart Materials and Structures* (SMS) and the *International Journal of Smart and Nano Materials* (TSNM).

Kam K. Leang (M'02) received the B.S. and M.S. degrees in mechanical engineering from the University of Utah, Salt Lake City, UT, USA, in 1997 and 1999, respectively, and the Ph.D. degree in mechanical engineering from the University of Washington, Seattle, WA, USA, in December 2004.

He is currently an Associate Professor in the Mechanical Engineering Department, University of Nevada—Reno, Reno, NV, USA, which he joined in 2008. His current research interests include modeling and control of piezoactuators for scanning probe microscopy applications, fabrication and control of electroactive polymers, and design and control of bioinspired autonomous systems.

Dr. Leang is an Associate Editor for the IEEE CONTROL SYSTEMS MAGAZINE and a Technical Editor for the IEEE/ASME TRANSACTIONS ON MECHATRONICS. He is also a member of the American Society of Mechanical Engineers (ASME) and the International Society for Optical Engineers (SPIE).